

The Direct and Generalized Linear Sampling Methods for Maxwell's Equations

Isaac Harris*

Dinh-Liem Nguyen[†]

Abstract

This paper is concerned with the inverse scattering problem that aims to determine the shape of electromagnetic scatterers from far field data (at a fixed frequency). We investigate the direct and generalized linear sampling methods for solving this electromagnetic inverse problem. Mathematical justifications of the sampling methods are provided. The Factorization method analysis for the far field operator plays an important role in these justifications. We prove the coercive property in the Factorization method for non-absorbing materials that allows us to follow the general framework of the generalized linear sampling method. The imaging functional for the direct sampling method is proposed and analyzed via a connection with the far field operator, the Factorization method analysis and the Funk-Hecke formula. Finally, we present some numerical examples to validate the performance of the direct sampling method.

Keywords. inverse electromagnetic scattering, direct sampling method, generalized linear sampling method, Maxwell's equations

AMS subject classification. 35R30, 35R09, 65R20

1 Introduction

In this paper, we consider the inverse shape problem that is derived from the time-harmonic electromagnetic scattering of an inhomogeneous medium. In many physical applications such as non-destructive testing and medical imaging one wishes to infer the shape and/or material properties of the scatterer from measured electromagnetic data. We assume that the far field measurements are known and we wish to analysis two sampling methods for recovering the scatterer. Sampling methods generally fall

*Department of Mathematics, Purdue University, West Lafayette, IN 47907; (harri814@purdue.edu)

[†]Department of Mathematics, Kansas State University, Manhattan, KS 66506; (dlnghuyen@ksu.edu)

under the category of qualitative (otherwise known as non-iterative or direct) reconstructive techniques. These methods are advantageous to use since they require little a-prior information to implement and are computationally simple. Qualitative methods have been used to solve multiple inverse shape problems as well as parameter identification in electromagnetic scattering (see for e.g. [4, 12] and the references therein). These methods have also been extended to inverse problems in the time domain. In [9] the Linear sampling method is applied to an inverse shape problem for heat conduction and in [6] the MUSIC algorithm is studied for recovering small volume scatterers for the time-dependent acoustic scattering problem. Here we rigorously analyze both the Direct sampling method and Generalized linear sampling method for recovering a penetrable inhomogeneous medium from electromagnetic far field data.

In general, sampling methods allow one to recover the scatterer by connecting the scatterer to the solution of a linear ill-posed equation involving the far field operator. Roughly speaking, the Linear sampling method gives that the so-called far field equation $\mathcal{F}g = \phi_{\mathbf{y}_s}$ is only solvable (via a regularization strategy) provided the sampling point is contained in the scatterer. Here the righthand side $\phi_{\mathbf{y}_s}$ is known and depends on the sampling point $\mathbf{y}_s \in \mathbb{R}^3$. This allows one to define an imaging functional that is the reciprocal of the norm of the solution to the far field equation which should only be non-zero as the regularization tends to zero for sampling points in the scatterer. See [4] for the analysis of the Linear sampling method for the electromagnetic scattering problem. The Factorization method gives that $\phi_{\mathbf{y}_s}$ is in the range of a positive self-adjoint compact operator defined by the far field operator if and only if the sampling point is in the scatterer. By appealing to Picard's criteria one can derive an imaging functional using the spectral decomposition of the far field operator see [12].

Recently, a new imaging functional given by the Direct sampling method has been studied in [14]. In this paper the Direct sampling method is shown to be equivalent to the Orthogonality sampling method proposed in [17]. Also in [8] the Direct sampling method is studied in connection to the spectral decomposition of the far field operator. The previous works in [8, 13, 14] all focus on acoustic scattering where we will extend the analysis to the case of electromagnetic scattering. This imaging functional is given by an inner-product only requiring the knowledge of $\phi_{\mathbf{y}_s}$ and the far field operator. By appealing to the known factorization of the far field operator it can be shown that the imaging functional is strictly positive and decays as the sampling point moves away from the scatterer. By appealing to the Funk-Hecke formula we are able to establish the decay rate. Since the Direct sampling method only requires one to compute the inner-product of known quantities this implies that it is computationally cheap to implement and stable in the presence of noise added to the far field data. One of the main contributions in this paper is the study of the symmetric factorization of the far field operator where the coercivity property of the middle operator is proven. Here we greatly reduce the regularity needed on the contrast to prove the coercivity estimate. We will also consider the Generalized linear sampling method for our inverse problem which was first developed in [1]. Here we will again use the factorization of the far

field operator to derive yet another imaging functional. The imaging functional here is derived from minimizing a residual in the far field equation with a penalty term that involves the inner-product of $\phi_{\mathbf{y}_s}$ and the far field operator. This method is motivated to rigorously connect the analysis of the Linear sampling and the Factorization methods.

We end this section by introducing some basic notations for the paper. Let $\mathcal{O} \subset \mathbb{R}^3$ be a domain (connected and open) with Lipschitz boundary, we indistinctly denote by (\cdot, \cdot) the inner product of $L^2(\mathcal{O})$ or $L^2(\mathcal{O})^3$ and by $\|\cdot\|$ the associated norms. We further denote

$$\begin{aligned} H(\text{curl}, \mathcal{O}) &= \{\mathbf{v} \in L^2(\mathcal{O})^3 : \text{curl } \mathbf{v} \in L^2(\mathcal{O})^3\}, \\ H_{\text{loc}}(\text{curl}, \mathbb{R}^3) &= \{\mathbf{v} : \mathbb{R}^3 \rightarrow \mathbb{C}^3 : \mathbf{v}|_B \in H(\text{curl}, B) \text{ for all ball } B \subset \mathbb{R}^3\}, \end{aligned}$$

where $H(\text{curl}, \mathcal{O})$ is equipped by usual inner product

$$(\cdot, \cdot)_{H(\text{curl}, \mathcal{O})} = (\text{curl } \cdot, \text{curl } \cdot) + (\cdot, \cdot).$$

For the following sections we will study the far field operator corresponding to the time-harmonic electromagnetic scattering of a penetrable media. First we will rigorously formulate the direct and inverse problem under consideration. We will then analyze the factorization of the far field operator to validate the Direct sampling method and Generalized linear sampling method. Lastly, numerical examples are given where we reconstruct bounded scatterers in \mathbb{R}^3 using the electromagnetic far field data. We see that the Direct sampling method is a robust reconstruction method that can recover scatterers of many different shapes and sizes.

2 Direct and inverse problem formulation

We consider the scattering of time-harmonic electromagnetic waves at positive frequency ω from a non-magnetic inhomogeneous medium. Suppose that there is with no free charge and current density. The electric field \mathbf{E} and the magnetic field \mathbf{H} are described by Maxwell's equations

$$\text{curl } \mathbf{E} - i\omega\mu_0\mathbf{H} = 0, \quad \text{curl } \mathbf{H} + i\omega\varepsilon\mathbf{E} = 0, \quad \text{in } \mathbb{R}^3, \quad (1)$$

where ε is the electric permittivity and μ_0 (positive constant) is the magnetic permeability of the medium. The permittivity ε is assumed to be a bounded function. Let Ω be a bounded domain occupied by the non-magnetic inhomogeneous medium. The medium outside of Ω is assumed to be homogeneous. This means that there is a positive constant ε_0 such that $\varepsilon = \varepsilon_0$ outside of Ω . We defined the relative material parameter and the wave number as

$$\varepsilon_r = \varepsilon/\varepsilon_0, \quad k = \omega\sqrt{\varepsilon_0\mu_0}.$$

Eliminating \mathbf{H} from (1) we obtain

$$\operatorname{curl} \operatorname{curl} \mathbf{E} - k^2 \varepsilon_r \mathbf{E} = 0, \quad \text{in } \mathbb{R}^3. \quad (2)$$

The transmission conditions across the boundary of Ω are given by

$$\nu \times \mathbf{E}_+ = \nu \times \mathbf{E}_-, \quad \nu \times \operatorname{curl} \mathbf{E}_+ = \nu \times \operatorname{curl} \mathbf{E}_-, \quad \text{on } \partial\Omega, \quad (3)$$

where \mathbf{F}_+ and \mathbf{F}_- are respectively the traces on $\partial\Omega$ from the exterior and interior of Ω for a vector function \mathbf{F} , and ν is an outward normal vector of Ω . Assume that we illuminate the inhomogeneous medium with incident electric and magnetic incident fields \mathbf{E}_{in} and \mathbf{H}_{in} , respectively, satisfying

$$\operatorname{curl} \mathbf{H}_{\text{in}} + i\omega \varepsilon_0 \mathbf{E}_{\text{in}} = 0, \quad \operatorname{curl} \mathbf{E}_{\text{in}} - i\omega \mu_0 \mathbf{H}_{\text{in}} = 0, \quad \text{in } \mathbb{R}^3.$$

Then there arises the scattered electric field \mathbf{u} , defined by $\mathbf{u} := \mathbf{E} - \mathbf{E}_{\text{in}}$. Since the incident field \mathbf{E}_{in} homogeneous Maxwell equation with wave number k given by

$$\operatorname{curl} \operatorname{curl} \mathbf{E}_{\text{in}} - k^2 \mathbf{E}_{\text{in}} = 0, \quad \text{in } \mathbb{R}^3$$

subtracting this equation from (2) we can conclude that the scattered field $\mathbf{u} \in H_{\text{loc}}(\operatorname{curl}, \mathbb{R}^3)$ is the solution to

$$\operatorname{curl} \operatorname{curl} \mathbf{u} - k^2 \varepsilon_r \mathbf{u} = k^2 P \mathbf{E}_{\text{in}} \quad \text{in } \mathbb{R}^3, \quad (4)$$

where the contrast P is defined by

$$P := \varepsilon_r - 1.$$

Therefore by definition we have that the support of the contrast P is given by Ω . Note that we also have corresponding transmission conditions for scattered field \mathbf{u} following from (3). We complete the scattering problem by the Silver-Müller radiation condition for the scattered field \mathbf{u} given by

$$\operatorname{curl} \mathbf{u} \times \frac{\mathbf{x}}{|\mathbf{x}|} - ik \mathbf{u} = \mathcal{O}(|\mathbf{x}|^{-2}) \quad \text{as } |\mathbf{x}| \rightarrow \infty, \quad (5)$$

which is assumed to hold uniformly with respect to \mathbf{x} .

It is known (see for e.g. [15]) that (4)–(5) is well-posed provided that the contrast P is bounded with non-negative real and imaginary parts with support Ω provided that the only solution to the homogeneous problem (i.e. $\mathbf{E}_{\text{in}} = 0$) is trivial. We will assume that the homogeneous scattering problem only admits the trivial solution. This gives that the mapping $\mathbf{E}_{\text{in}} \mapsto \mathbf{u}$ is linear and bounded from $L^2(\Omega)^3$ into $H_{\text{loc}}(\operatorname{curl}, \mathbb{R}^3)$.

Now we can talk about the inverse problem. To this end, we define $\widehat{\mathbf{x}} = \mathbf{x}/|\mathbf{x}|$,

$$\mathbb{S}^2 = \{\mathbf{x} \in \mathbb{R}^3 : |\mathbf{x}| = 1\} \quad \text{and} \quad L_t^2(\mathbb{S}^2) = \{\mathbf{v} \in L^2(\mathbb{S}^2)^3 : \widehat{\mathbf{x}} \cdot \mathbf{v}(\widehat{\mathbf{x}}) = 0, \widehat{\mathbf{x}} \in \mathbb{S}^2\}.$$

We consider the incident plane wave $\mathbf{E}_{\text{in}}(\mathbf{x}, \mathbf{d}, \mathbf{q}) = \mathbf{q}e^{ik\mathbf{x}\cdot\mathbf{d}}$, where the vector $\mathbf{d} \in \mathbb{S}^2$ indicates the direction of the incident propagation and $\mathbf{q} \in \mathbb{R}^3$ is the polarization vector such that $\mathbf{q} \cdot \mathbf{d} = 0$. It's well-known that we can express the corresponding scattered wave in terms of the asymptotic expansion

$$\mathbf{u}(\mathbf{x}, \mathbf{d}, \mathbf{q}) = \frac{e^{ik|\mathbf{x}|}}{|\mathbf{x}|} \left(\mathbf{u}^\infty(\widehat{\mathbf{x}}, \mathbf{d}, \mathbf{q}) + O\left(\frac{1}{|\mathbf{x}|^2}\right) \right), \quad |\mathbf{x}| \rightarrow \infty,$$

uniformly in all directions $\widehat{\mathbf{x}} \in \mathbb{S}^2$. The function $\mathbf{u}^\infty(\widehat{\mathbf{x}}, \mathbf{d}, \mathbf{q})$ which belongs to $L_t^2(\mathbb{S}^2)$ is called far field pattern.

Inverse problem: Determine the shape and location of the scatterer Ω given the far field pattern $\mathbf{u}^\infty(\widehat{\mathbf{x}}, \mathbf{d}, \mathbf{q})$ for all $\widehat{\mathbf{x}}, \mathbf{d} \in \mathbb{S}^2$ for a single wave number.

3 The far field operator and generalized linear sampling method

In this section, we will define and analyze the far field operator corresponding to (4)–(5). The analysis in this section will be used to derive sampling methods to solve the inverse shape problem of recovering the scatterer Ω from the far field data. The analysis in this section is motivated by the coercivity result in [1] where we extend this analysis to the case of electromagnetic scattering.

It is well-known that the far field pattern $\mathbf{u}^\infty(\widehat{\mathbf{x}}, \mathbf{d}, \mathbf{q})$ is linear in \mathbf{q} and can be written as

$$\mathbf{u}^\infty(\widehat{\mathbf{x}}, \mathbf{d}, \mathbf{q}) = \mathbf{u}^\infty(\widehat{\mathbf{x}}, \mathbf{d})\mathbf{q}$$

where $\mathbf{u}^\infty(\widehat{\mathbf{x}}, \mathbf{d})$ is a 3×3 matrix and $\mathbf{q} \cdot \mathbf{d} = 0$, see for e.g. [7, page 224]. The following reciprocity relation is important in our analysis and its proof can be found in [7, Theorem 6.30].

Theorem 1. *For all $\widehat{\mathbf{x}}, \mathbf{d} \in \mathbb{S}^2$, the far field pattern $\mathbf{u}^\infty(\widehat{\mathbf{x}}, \mathbf{d})$ satisfies a reciprocity relation*

$$\mathbf{u}^\infty(\widehat{\mathbf{x}}, \mathbf{d}) = [\mathbf{u}^\infty(-\mathbf{d}, -\widehat{\mathbf{x}})]^\top.$$

We now define the far field operator $\mathcal{F} : L_t^2(\mathbb{S}^2) \rightarrow L_t^2(\mathbb{S}^2)$ as

$$(\mathcal{F}\mathbf{g})(\widehat{\mathbf{x}}) = \int_{\mathbb{S}^2} \mathbf{u}^\infty(\widehat{\mathbf{x}}, \mathbf{d})\mathbf{g}(\mathbf{d})ds(\mathbf{d}).$$

In order to derive our sampling methods we will need to factorize the operator the far field operator \mathcal{F} . To this end, it has been shown in [11] that the far field operator has the following factorization $\mathcal{F} = GH$. Here the operator

$$H : L_t^2(\mathbb{S}^2) \rightarrow L^2(\Omega)^3 \text{ is given by } (H\mathbf{g})(\mathbf{x}) = \int_{\mathbb{S}^2} \mathbf{g}(\mathbf{d})e^{ik\mathbf{x}\cdot\mathbf{d}}ds(\mathbf{d}), \quad \mathbf{x} \in \Omega \quad (6)$$

and is the superposition of incident plane waves. It is easy to see that H is compact and injective. The data to far field pattern operator

$$G : L^2(\Omega)^3 \rightarrow L_t^2(\mathbb{S}^2) \quad \text{is given by} \quad G\mathbf{f} = \mathbf{v}^\infty \quad (7)$$

where $\mathbf{v} \in H_{\text{loc}}(\text{curl}, \mathbb{R}^3)$ is the solution to (4)–(5) with $\mathbf{E}_{\text{in}} = \mathbf{f}$. The adjoint operator H^* of H is given by

$$H^*\mathbf{f}(\mathbf{d}) = \mathbf{d} \times \left(\int_{\Omega} \mathbf{f}(\mathbf{x}) e^{-ik\mathbf{x}\cdot\mathbf{d}} d\mathbf{x} \right) \times \mathbf{d}, \quad \mathbf{d} \in \mathbb{S}^2.$$

From the form of the data to far field pattern operator a factorization of G in [11] gives that $G = H^*T$ with

$$T : L^2(\Omega)^3 \rightarrow L^2(\Omega)^3 \quad \text{is given by} \quad (T\mathbf{f})(\mathbf{x}) = k^2 P(\mathbf{f} + \mathbf{v}) \quad (8)$$

where again $\mathbf{v} \in H_{\text{loc}}(\text{curl}, \mathbb{R}^3)$ is the solution to (4)–(5) with $\mathbf{E}_{\text{in}} = \mathbf{f}$. Due to the well-posedness of the direct problem and the boundedness of P it is clear that T is a bounded operator on $L^2(\Omega)^3$, and hence $G = H^*T$ is also a compact operator. This gives that $\mathcal{F} = H^*TH$. This factorization is used to derive the Factorization method for reconstruction Ω in [11]. In order to continue we first make the following assumptions on the domain and coefficients.

Assumption 2. *We will assume that Ω is a simply connected bounded subset of \mathbb{R}^3 with $\partial\Omega$ being class C^2 . For an absorbing material we assume $P \in L^\infty(\Omega)$ and for a non-absorbing material we assume $P \in L^\infty(\Omega) \cap H_0^1(\Omega)$. Where $H_0^1(\Omega)$ is the standard Sobolev space of L^2 functions with a weak gradient in L^2 and zero trace on $\partial\Omega$.*

Note that extra regularity is also needed for the case of a non-absorbing material in [11] when analyzing the Factorization method but the regularity here is much weaker. The assumption that the contrast be in $L^\infty(\Omega) \cap H_0^1(\Omega)$ gives that it is bounded in Ω which is required for the forward scattering problem (4)–(5) and an L^2 gradient which will be needed in our analysis. We lastly assume that the wave number k is not a transmission eigenvalue i.e. the only solution to the homogeneous system in $L^2(\Omega)^3 \times L^2(\Omega)^3$

$$\text{curl curl } \mathbf{w} - k^2 \varepsilon_r \mathbf{w} = 0 \quad \text{and} \quad \text{curl curl } \boldsymbol{\varphi} - k^2 \boldsymbol{\varphi} = 0 \quad \text{in } \Omega \quad (9)$$

$$\boldsymbol{\nu} \times \mathbf{w} = \boldsymbol{\nu} \times \boldsymbol{\varphi} \quad \text{and} \quad \boldsymbol{\nu} \times \text{curl } \mathbf{w} = \boldsymbol{\nu} \times \text{curl } \boldsymbol{\varphi} \quad \text{on } \partial\Omega \quad (10)$$

is trivial. It is known that the set of real transmission eigenvalues is at most discrete for a real-valued permittivity and is empty for a complex valued permittivity. See [5] and the references therein for the analysis of transmission eigenvalue problems.

The following results can be found in [11]. These results will be critical in the later sections where we study the Direct sampling method and Generalized linear sampling method.

Theorem 3. *Let the operators H and T be as defined in (6)–(8) and let $\mathbf{p}, \mathbf{y}_s \in \mathbb{R}^3$.*

- a. The operator H is compact and injective.*
- b. The far field operator \mathcal{F} is compact, injective and has dense range.*
- c. The far field operator has the factorization $\mathcal{F} = GH$ where $G = H^*T$.*
- d. The operator T is coercive on $L^2(\Omega)^3$ provided the imaginary part of P is positive definite.*
- e. Let $\phi_{\mathbf{y}_s}(\mathbf{d}) = (\mathbf{d} \times \mathbf{p}) \times \mathbf{d} e^{-ik\mathbf{d} \cdot \mathbf{y}_s}$ then $\phi_{\mathbf{y}_s} \in \text{Range}(H^*) \iff \mathbf{y}_s \in \Omega$.*

Even though we assume that the contrast is given by a scalar function we have that Theorem 3 is valid for a matrix-valued contrast provided that its entries are in $L^\infty(\Omega)$. As we will see the above factorization as well as the coercivity of the middle operator T are the crucial components in our analysis of the sampling methods we propose to solve the inverse problem. Therefore, the sampling methods studied here are still valid of a matrix-valued contrast provided that the imaginary part is a positive definite matrix.

The main piece that is missing for developing the sampling methods in the proceeding sections is the coercivity of the operator T for a non-absorbing material. To this end, we now prove a coercivity result for a real-valued contrast $P \in L^\infty(\Omega) \cap H_0^1(\Omega)$. For our analysis it is sufficient to prove coercivity on the closure of the $\text{Range}(H)$ which is the space of $L^2(\Omega)^3$ solutions to the homogeneous Maxwell equation with wave number k (see for e.g. [4]) i.e.

$$\varphi \in \overline{\text{Range}(H)} \iff \text{curl curl } \varphi - k^2 \varphi = 0 \quad \text{a.e. in } \Omega.$$

Here the Maxwell equation is understood in the ultra weak sense where $\varphi \in L^2(\Omega)^3$ is a solution with wave number k if

$$\int_{\Omega} \varphi \cdot (\text{curl curl } \psi - k^2 \psi) \, d\mathbf{x} = 0$$

for every smooth vector field ψ supported in Ω . Also the $L^2(\Omega)^3 \times L^2(\Omega)^3$ solutions to the transmission eigenvalue (9)–(10) are understood in the ultra weak sense.

We now recall the global Div-Curl lemma given in [18].

Lemma 4 (global Div-Curl lemma). *Let φ_j and ψ_j be vector-valued sequences that converge weakly in $L^2(\Omega)^3$ to φ and ψ respectively. Assume that*

$$\|\nabla \cdot \varphi_j\| \leq C \quad \text{and} \quad \|\text{curl } \psi_j\| \leq C \quad \text{for every } j \in \mathbb{N}.$$

Further assume that either

$$\varphi_j \cdot \nu = 0 \quad \text{or} \quad \psi_j \times \nu = 0 \quad \text{on } \partial\Omega.$$

Then

$$\int_{\Omega} \varphi_j \cdot \psi_j \, d\mathbf{x} \rightarrow \int_{\Omega} \varphi \cdot \psi \, d\mathbf{x} \quad \text{as } j \rightarrow \infty.$$

With this we are now ready to prove the coercivity estimate for a real valued contrast. This lemma is the key component in our analysis that is what is needed to reduce the regularity assumptions on the contrast.

Theorem 5. *Let the operator T be as defined in (8). If $P \in L^\infty(\Omega) \cap H_0^1(\Omega)$ satisfies $P \geq p_0 > 0$ a.e. in Ω and k is not a transmission eigenvalue then T is coercive on $\overline{\text{Range}(H)}$.*

Proof. Notice, that by the definition of T we have that

$$(T\mathbf{f}, \mathbf{f}) = k^2 \int_{\Omega} P(\mathbf{f} + \mathbf{v})\bar{\mathbf{f}} \, d\mathbf{x}.$$

By appealing to (4)–(5) one can show with Green’s Theorem that (see [11])

$$(T\mathbf{f}, \mathbf{f}) = k^2 \int_{\Omega} P|\mathbf{f} + \mathbf{v}|^2 \, d\mathbf{x} - \int_{\Omega} |\text{curl } \mathbf{v}|^2 - k^2|\mathbf{v}|^2 \, d\mathbf{x} + ik \int_{\mathbb{S}^2} |\mathbf{v}^\infty|^2 ds(\mathbf{d})$$

where \mathbf{v}^∞ is the far field pattern of \mathbf{v} . The integral over \mathbb{S}^2 comes from applying the radiation condition and using the asymptotics of the scattered wave \mathbf{v} with respect to the far field pattern.

Now assume that T is not coercive in $\overline{\text{Range}(H)}$, this implies that there is a sequence $\mathbf{f}_j \in \overline{\text{Range}(H)}$ such that $\|\mathbf{f}_j\| = 1$ for all $j \in \mathbb{N}$ where $|(T\mathbf{f}_j, \mathbf{f}_j)| \rightarrow 0$ as $j \rightarrow \infty$. We have that there is a $\mathbf{f} \in L^2(\Omega)^3$ that satisfies the homogeneous Maxwell equation with wave number k that is the weak limit of \mathbf{f}_j up to a subsequence. Similarly by the well-posedness of (4)–(5) we have that there is a $\mathbf{v} \in H_{\text{loc}}(\text{curl}, \mathbb{R}^3)$ that is the corresponding weak limit of \mathbf{v}_j up to a subsequence. By the compactness of G we can conclude that the far field pattern $\mathbf{v}_j^\infty \rightarrow \mathbf{v}^\infty$ in the $L^2(\mathbb{S}^2)$ norm where \mathbf{v}^∞ is the far field pattern for the limiting solution \mathbf{v} . Since

$$\text{Im}(T\mathbf{f}_j, \mathbf{f}_j) = k \int_{\mathbb{S}^2} |\mathbf{v}_j^\infty|^2 ds(\mathbf{d}) \rightarrow 0 \quad \text{as } j \rightarrow \infty$$

we can conclude that $\mathbf{v}^\infty = 0$ and therefore $\mathbf{v} = 0$ in the exterior of Ω (see for e.g. [4]). This implies that $(\mathbf{v} + \mathbf{f}, \mathbf{f}) \in L^2(\Omega)^3 \times L^2(\Omega)^3$ are a pair of transmission eigenfunctions which implies that $\mathbf{v} = \mathbf{f} = 0$ in Ω since we have assumed that k is not a transmission eigenvalue. We have that \mathbf{v}_j weakly converges to the zero vector and by the well-posedness has a curl that is bounded uniformly with respect to $j \in \mathbb{N}$. We also have that $P\mathbf{f}_j$ weakly converges to the zero vector and that

$$\nabla \cdot (P\mathbf{f}_j) = (\nabla P) \cdot \mathbf{f}_j \quad \text{since} \quad \text{curl curl } \mathbf{f}_j - k^2\mathbf{f}_j = 0 \quad \text{a.e. in } \Omega.$$

By our assumption that $P \in L^\infty(\Omega) \cap H_0^1(\Omega)$ we conclude that the divergence of $P\mathbf{f}_j$ is bounded uniformly with respect to $j \in \mathbb{N}$ by

$$\|\nabla \cdot (P\mathbf{f}_j)\| \leq \|\nabla P\| \|\mathbf{f}_j\| \leq C\|P\|_{H^1(\Omega)}$$

and $(P\mathbf{f}_j) \cdot \nu = 0$ on $\partial\Omega$ by the zero trace of the contrast. Since $P \geq p_0 > 0$ a.e. in Ω then by the triangle inequality

$$|(T\mathbf{f}_j, \mathbf{f}_j)| \geq k^2 p_0 \int_{\Omega} |\mathbf{f}_j|^2 dx - k^2 \left| \int_{\Omega} \mathbf{v}_j \cdot P\overline{\mathbf{f}_j} dx \right|.$$

By appealing to Lemma 4 (global Div-Curl lemma) we have that

$$k^2 p_0 \leq \lim_{j \rightarrow \infty} |(T\mathbf{f}_j, \mathbf{f}_j)| = 0$$

which contradicts the fact the $k^2 p_0$ is positive. The above analysis gives the result. \square

The result given in Theorem 5 will be instrumental to the coming sections. Also, this coercivity result requires less regularity than what is need for the Factorization method. From the remark in section 5 of [11] their restrictions on P excludes the case of a homogeneous spherical scatterer. Since here we only require $P \in L^\infty(\Omega) \cap H_0^1(\Omega)$ and strictly positive we have that our sampling methods will be justified of a wide range of scatterers.

Here we extend the analysis in [1] to the case of an electromagnetic scatterer. Recently, an alternative mathematically rigors sampling method has been introduced in [1] referred to as Generalized linear sampling method (GLSM). Just as the work in [2] and [3] this sampling method was developed to bridge theoretical gap between the Linear sampling and the Factorization methods. Using the factorizations given in section 3 we can connect the support of Ω to the solution of a minimization problem. The GLSM considers the problem of finding a minimizer for $\mathcal{J}(\cdot; \alpha) : L_t^2(\mathbb{S}^2) \rightarrow \mathbb{R}$ where the functional

$$\mathcal{J}(g; \alpha) = \alpha \left| \langle \mathcal{F}g, g \rangle_{L_t^2(\mathbb{S}^2)} \right| + \|\mathcal{F}g - \phi_{\mathbf{y}_s}\|_{L_t^2(\mathbb{S}^2)}^2 \quad (11)$$

for any parameter $\alpha > 0$.

In the functional $\mathcal{J}(\cdot; \alpha)$ the term $\left| \langle \mathcal{F}g, g \rangle_{L_t^2(\mathbb{S}^2)} \right|$ acts as a penalizing term that is motivated from the Linear sampling method. Let the minimizing sequence as $\alpha \rightarrow 0$ be denoted as $g_{\mathbf{y}_s}^\alpha$. Due to the factorization and coercivity results in Theorems 3 and 5 we have that the term $\left| \langle \mathcal{F}g_{\mathbf{y}_s}^\alpha, g_{\mathbf{y}_s}^\alpha \rangle_{L_t^2(\mathbb{S}^2)} \right|$ is equivalent to $\|Hg_{\mathbf{y}_s}^\alpha\|^2$ which is only bounded as $\alpha \rightarrow 0$ for $\mathbf{y}_s \in \Omega$ provided that $\|\mathcal{F}g_{\mathbf{y}_s}^\alpha - \phi_{\mathbf{y}_s}\|_{L_t^2(\mathbb{S}^2)} \rightarrow 0$ as $\alpha \rightarrow 0$. We now prove that determining $g_{\mathbf{y}_s}^\alpha$ can be used to recover the scatterer.

Theorem 6. *Assume that there is a $C > 0$ independent of α such that*

$$\mathcal{J}(g_{\mathbf{y}_s}^\alpha; \alpha) \leq \inf_{L_t^2(\mathbb{S}^2)} \mathcal{J}(\cdot; \alpha) + C\alpha$$

where $g_{\mathbf{y}_s}^\alpha$ denotes a minimizing sequence of (11).

$$\text{Then } \mathbf{y}_s \in \Omega \iff \liminf_{\alpha \rightarrow 0} \left| \langle \mathcal{F}g_{\mathbf{y}_s}^\alpha, g_{\mathbf{y}_s}^\alpha \rangle_{L_t^2(\mathbb{S}^2)} \right| < \infty.$$

Proof. This is a direct application of Theorem 3 in [1] and the analysis in chapter 4 of [4]. \square

Since in many applications the far field operator is only known up to a perturbation. This gives that the measured far field operator \mathcal{F}^δ is such that

$$\|\mathcal{F} - \mathcal{F}^\delta\|_{L_t^2(\mathbb{S}^2) \rightarrow L_t^2(\mathbb{S}^2)} \leq \delta$$

where δ is the norm of the perturbation. In this case one considers the regularized version of (11) which is given by

$$\mathcal{J}^\delta(g; \alpha) = \alpha \left(|\langle \mathcal{F}^\delta g, g \rangle_{L_t^2(\mathbb{S}^2)}| + \delta \|g\|_{L_t^2(\mathbb{S}^2)}^2 \right) + \|\mathcal{F}^\delta g - \phi_{\mathbf{y}_s}\|_{L_t^2(\mathbb{S}^2)}^2 \quad (12)$$

where the parameter $\alpha > 0$. We denote the minimizer of the regularized functional (12) by $g_{\mathbf{y}_s}^{\alpha, \delta}$. Similarly to the unperturbed case we have the following result.

Theorem 7. *Assume that the unperturbed minimization problem satisfies the assumptions of Theorem 6 and let $g_{\mathbf{y}_s}^\alpha$ denotes the minimizer of (12).*

$$\text{Then } \mathbf{y}_s \in \Omega \iff \liminf_{\alpha \rightarrow 0} \liminf_{\delta \rightarrow 0} \left(|\langle \mathcal{F}^\delta g_{\mathbf{y}_s}^{\alpha, \delta}, g_{\mathbf{y}_s}^{\alpha, \delta} \rangle_{L_t^2(\mathbb{S}^2)}| + \delta \|g_{\mathbf{y}_s}^{\alpha, \delta}\|_{L_t^2(\mathbb{S}^2)}^2 \right) < \infty.$$

Proof. See [1] section 3 for details. \square

The above results give another way to recover the scatterer Ω from the scattering data. By Theorem 6 gives a new imaging functional, where one plots the reciprocal of function $\mathbf{y}_s \mapsto |\langle \mathcal{F} g_{\mathbf{y}_s}^\alpha, g_{\mathbf{y}_s}^\alpha \rangle_{L_t^2(\mathbb{S}^2)}|$ to recover the scatterer. In the case where there is noise added to the scattering data the indicator function given by Theorem 7 is

$$\mathbf{y}_s \longmapsto \frac{1}{|\langle \mathcal{F}^\delta g_{\mathbf{y}_s}^{\alpha, \delta}, g_{\mathbf{y}_s}^{\alpha, \delta} \rangle_{L_t^2(\mathbb{S}^2)}| + \delta \|g_{\mathbf{y}_s}^{\alpha, \delta}\|_{L_t^2(\mathbb{S}^2)}^2}$$

where $g_{\mathbf{y}_s}^{\alpha, \delta}$ denotes the minimizer of (12). In order to compute the minimizer of the functional $\mathcal{J}^\delta(\cdot; \alpha)$ one can appeal to an iterative method where the initial guess is given by the Linear sampling method and the regularization parameter $\alpha(\delta)$ is given by Morozov discrepancy principle for the Tikhonov regularization functional.

4 Direct sampling method

This section is dedicated to studying the Direct sampling method for reconstructing the scatterer Ω . The analysis in this section is motivated by the work in [14] where a new imaging functional is presented and studied for the inverse acoustic scattering problem. In [14] the analysis given by the Factorization method as well as the Funk-Hecke formula is used to show that the imaging functional is bounded below and decays as $\text{dist}(\mathbf{y}_s, \Omega)$ increases where \mathbf{y}_s is the sampling point. Similar techniques are used

in [10] to show that a similar imaging functionals can be used recover a Dirichlet or Neumann obstacle for the case of elastic scattering data. Here we extend this idea to electromagnetic scatterers using the factorization discussed in the previous section.

The imaging functional. We are interested in imaging of the scatterer Ω given the far field pattern $\mathbf{u}^\infty(\widehat{\mathbf{x}}, \mathbf{d}, \mathbf{q})$, for all $\widehat{\mathbf{x}}, \mathbf{d} \in \mathbb{S}^2$ given by the polarization vector $\mathbf{q} = (\mathbf{d} \times \mathbf{p}) \times \mathbf{d}$. Let \mathbf{y}_s be the sampling points in the imaging process and $\mathbf{p} \in \mathbb{R}^3$ is a fixed vector. We define the imaging functional \mathcal{I} as

$$\mathcal{I}(\mathbf{y}_s) := \left| \int_{\mathbb{S}^2} e^{-ik\mathbf{d}\cdot\mathbf{y}_s} \int_{\mathbb{S}^2} \mathbf{u}^\infty(\widehat{\mathbf{x}}, \mathbf{d})(\mathbf{d} \times \mathbf{p}) \times \mathbf{d} \cdot ((\widehat{\mathbf{x}} \times \mathbf{p}) \times \widehat{\mathbf{x}} e^{ik\widehat{\mathbf{x}}\cdot\mathbf{y}_s}) ds(\widehat{\mathbf{x}}) ds(\mathbf{d}) \right|. \quad (13)$$

The use of $(\mathbf{d} \times \mathbf{p}) \times \mathbf{d}$ in the imaging functional is to have the polarization vector belonging to $L_t^2(\mathbb{S}^2)$ for any choice of $\mathbf{p} \in \mathbb{R}^3$. This allowed us to write the far field pattern as a matrix vector product. We now wish to write the imaging functional in terms of the far field operator. This will allow us to study the the imaging functional using the factorization in the previous section.

Lemma 8. *The functional \mathcal{I} defined in (13) satisfies*

$$\mathcal{I}(\mathbf{y}_s) = \left| \langle \mathcal{F}\phi_{\mathbf{y}_s}, \phi_{\mathbf{y}_s} \rangle_{L_t^2(\mathbb{S}^2)} \right|$$

where again $\phi_{\mathbf{y}_s} \in L_t^2(\mathbb{S}^2)$ is given by

$$\phi_{\mathbf{y}_s}(\mathbf{d}) = (\mathbf{d} \times \mathbf{p}) \times \mathbf{d} e^{-ik\mathbf{d}\cdot\mathbf{y}_s}.$$

Proof. We use the reciprocity relation and interchange the roles of $\widehat{\mathbf{x}}$ and \mathbf{d}

$$\begin{aligned} \mathcal{I}(\mathbf{y}_s) &= \left| \int_{\mathbb{S}^2} e^{-ik\mathbf{d}\cdot\mathbf{y}_s} \int_{\mathbb{S}^2} \mathbf{u}^\infty(\widehat{\mathbf{x}}, \mathbf{d})(\mathbf{d} \times \mathbf{p}) \times \mathbf{d} \cdot ((\widehat{\mathbf{x}} \times \mathbf{p}) \times \widehat{\mathbf{x}} e^{ik\widehat{\mathbf{x}}\cdot\mathbf{y}_s}) ds(\widehat{\mathbf{x}}) ds(\mathbf{d}) \right| \\ &= \left| \int_{\mathbb{S}^2} e^{-ik\mathbf{d}\cdot\mathbf{y}_s} \int_{\mathbb{S}^2} [\mathbf{u}^\infty(-\mathbf{d}, -\widehat{\mathbf{x}})]^\top (\mathbf{d} \times \mathbf{p}) \times \mathbf{d} \cdot ((\widehat{\mathbf{x}} \times \mathbf{p}) \times \widehat{\mathbf{x}} e^{ik\widehat{\mathbf{x}}\cdot\mathbf{y}_s}) ds(\widehat{\mathbf{x}}) ds(\mathbf{d}) \right| \\ &= \left| \int_{\mathbb{S}^2} \int_{\mathbb{S}^2} [\mathbf{u}^\infty(\mathbf{d}, \widehat{\mathbf{x}})]^\top (\mathbf{d} \times \mathbf{p}) \times \mathbf{d} e^{ik\mathbf{d}\cdot\mathbf{y}_s} \cdot ((\widehat{\mathbf{x}} \times \mathbf{p}) \times \widehat{\mathbf{x}} e^{-ik\widehat{\mathbf{x}}\cdot\mathbf{y}_s}) ds(\widehat{\mathbf{x}}) ds(\mathbf{d}) \right| \\ &= \left| \int_{\mathbb{S}^2} \int_{\mathbb{S}^2} \mathbf{u}^\infty(\mathbf{d}, \widehat{\mathbf{x}})(\widehat{\mathbf{x}} \times \mathbf{p}) \times \widehat{\mathbf{x}} e^{-ik\widehat{\mathbf{x}}\cdot\mathbf{y}_s} \cdot ((\mathbf{d} \times \mathbf{p}) \times \mathbf{d} e^{ik\mathbf{d}\cdot\mathbf{y}_s}) ds(\widehat{\mathbf{x}}) ds(\mathbf{d}) \right| \\ &= \left| \int_{\mathbb{S}^2} \int_{\mathbb{S}^2} \mathbf{u}^\infty(\widehat{\mathbf{x}}, \mathbf{d})(\mathbf{d} \times \mathbf{p}) \times \mathbf{d} e^{-ik\mathbf{d}\cdot\mathbf{y}_s} ds(\mathbf{d}) \cdot ((\widehat{\mathbf{x}} \times \mathbf{p}) \times \widehat{\mathbf{x}} e^{ik\widehat{\mathbf{x}}\cdot\mathbf{y}_s}) ds(\widehat{\mathbf{x}}) \right| \\ &= \left| \langle \mathcal{F}\phi_{\mathbf{y}_s}, \phi_{\mathbf{y}_s} \rangle_{L_t^2(\mathbb{S}^2)} \right| \end{aligned}$$

proving the claim. \square

Now that we have shown that the imaging functional can be represented by the inner product of the far field operator and the function $\phi_{\mathbf{y}_s}$ we now turn our attention

to studying its properties. Just as in the previous section we will assume that for an absorbing material $P \in L^\infty(\Omega)$ with uniformly positive imaginary part and for a non-absorbing material $P \in L^\infty(\Omega) \cap H_0^1(\Omega)$ is uniformly positive.

Theorem 9. *For every $\mathbf{y}_s \in \Omega$ the imaging functional $\mathcal{I}(\mathbf{y}_s)$ is bounded from below by a positive constant. Moreover, for $\mathbf{y}_s \notin \Omega$ the imaging functional satisfies*

$$\mathcal{I}(\mathbf{y}_s) = O\left(\frac{1}{\text{dist}(\mathbf{y}_s, \Omega)^2}\right), \quad \text{as } \text{dist}(\mathbf{y}_s, \Omega) \rightarrow \infty.$$

Proof. From Theorem 3 and Lemma 8 we have

$$\mathcal{I}(\mathbf{y}_s) = |\langle \mathcal{F}\phi_{\mathbf{y}_s}, \phi_{\mathbf{y}_s} \rangle_{L_t^2(\mathbb{S}^2)}| = |\langle H^*TH\phi_{\mathbf{y}_s}, \phi_{\mathbf{y}_s} \rangle_{L_t^2(\mathbb{S}^2)}| = |\langle TH\phi_{\mathbf{y}_s}, H\phi_{\mathbf{y}_s} \rangle_{L_t^2(\mathbb{S}^2)}|.$$

The Cauchy-Schwarz inequality and the coercivity of T in Theorem 5 implies that there are positive constants c_1 and c_2 such that

$$c_1 \|H\phi_{\mathbf{y}_s}\|^2 \leq \mathcal{I}(\mathbf{y}_s) \leq c_2 \|H\phi_{\mathbf{y}_s}\|^2.$$

Let $\mathbf{y}_s \in \Omega$. Then $\phi_{\mathbf{y}_s} \in \text{Range}(H^*)$ by Theorem 3. Therefore, we have $\phi_{\mathbf{y}_s} = H^*\varphi_{\mathbf{y}_s}$ for some $\varphi_{\mathbf{y}_s} \neq 0$, and

$$\begin{aligned} \|H\phi_{\mathbf{y}_s}\| &= \frac{\|H\phi_{\mathbf{y}_s}\| \|\varphi_{\mathbf{y}_s}\|}{\|\varphi_{\mathbf{y}_s}\|} \\ &\geq \frac{\langle H\phi_{\mathbf{y}_s}, \varphi_{\mathbf{y}_s} \rangle}{\|\varphi_{\mathbf{y}_s}\|} \\ &= \frac{\langle \phi_{\mathbf{y}_s}, H^*\varphi_{\mathbf{y}_s} \rangle}{\|\varphi_{\mathbf{y}_s}\|} = \frac{\|\phi_{\mathbf{y}_s}\|^2}{\|\varphi_{\mathbf{y}_s}\|} > 0. \end{aligned}$$

We now show that the imaging functional decays as $\text{dist}(\mathbf{y}_s, \Omega) \rightarrow \infty$. To do so, we can show that $\|H\phi_{\mathbf{y}_s}\|^2$ satisfies the decay property and use the upper bound on the imaging functional given above. Here we let Y_ℓ^m denote the spherical harmonics which form a complete orthonormal system on $L^2(\mathbb{S}^2)$. Now, recall the Funk-Hecke formula (see for e.g. [7])

$$\int_{\mathbb{S}^2} Y_\ell^m(\mathbf{d}) e^{-ik\mathbf{d}\cdot\mathbf{x}} dS(\mathbf{d}) = \frac{4\pi}{i^\ell} Y_\ell^m(\hat{\mathbf{x}}) j_\ell(k|\mathbf{x}|) \quad \text{for } m \in \mathbb{N} \cup \{0\} \text{ and } \ell = -m, \dots, m$$

where j_ℓ is the first kind spherical Bessel function of order ℓ . In particular,

$$Y_0^0 = \frac{1}{\sqrt{4\pi}}, \quad j_0(t) = \frac{\sin(t)}{t}.$$

Just as in recent works [8, 16] we will use the Funk-Hecke formula to show that $\|H\phi_{\mathbf{y}_s}\|^2$ decays as $\text{dist}(\mathbf{y}_s, \Omega) \rightarrow \infty$. Indeed, using the Funk-Hecke formula for $m = \ell = 0$, the

formula $\text{curl}_{\mathbf{z}} \text{curl}_{\mathbf{z}}(\mathbf{p}e^{-ik\mathbf{d}\cdot\mathbf{z}}) = -k^2(\mathbf{d} \times \mathbf{p}) \times \mathbf{d}e^{-ik\mathbf{d}\cdot\mathbf{z}}$ and straightforward calculations we have (see [16] for details)

$$\begin{aligned} \int_{\mathbb{S}^2} (\mathbf{d} \times \mathbf{p}) \times \mathbf{d}e^{-ik\mathbf{d}\cdot\mathbf{z}} ds(\mathbf{d}) &= -\frac{1}{k^2} \text{curl}_{\mathbf{z}} \text{curl}_{\mathbf{z}} \int_{\mathbb{S}^2} \mathbf{p}e^{-ik\mathbf{d}\cdot\mathbf{z}} ds(\mathbf{d}) \\ &= -\frac{4\pi}{k^2} \text{curl}_{\mathbf{z}} \text{curl}_{\mathbf{z}}(\mathbf{p}j_0(k|\mathbf{z}|)) = -\frac{4\pi}{k^2} \begin{pmatrix} v_1(\mathbf{z}, \mathbf{p}) \\ v_2(\mathbf{z}, \mathbf{p}) \\ v_3(\mathbf{z}, \mathbf{p}) \end{pmatrix} \end{aligned}$$

where, for $j = 1, 2, 3$,

$$v_j(\mathbf{z}, \mathbf{p}) = k^2 \left(\frac{|\mathbf{z}|^2 - (\mathbf{p} \cdot \mathbf{z})z_j}{|\mathbf{z}|^2} \right) j_0(k|\mathbf{z}|) - 3 \left(\frac{(\mathbf{p} \cdot \mathbf{z})z_j}{|\mathbf{z}|^4} \right) (\cos(k|\mathbf{z}|) - j_0(k|\mathbf{z}|)).$$

It is obvious that $v_j = O(1/|\mathbf{z}|)$ as $|\mathbf{z}| \rightarrow \infty$. Therefore

$$(H\phi_{\mathbf{y}_s})(\mathbf{x}) = \int_{\mathbb{S}^2} (\mathbf{d} \times \mathbf{p}) \times \mathbf{d}e^{-ik\mathbf{d}\cdot(\mathbf{y}_s - \mathbf{x})} ds(\mathbf{d}) = -\frac{4\pi}{k^2} \begin{pmatrix} v_1(\mathbf{y}_s - \mathbf{x}, \mathbf{p}) \\ v_2(\mathbf{y}_s - \mathbf{x}, \mathbf{p}) \\ v_3(\mathbf{y}_s - \mathbf{x}, \mathbf{p}) \end{pmatrix}$$

which leads to

$$\|H\phi_{\mathbf{y}_s}\|^2 = O\left(\frac{1}{\text{dist}(\mathbf{y}_s, \Omega)^2}\right), \quad \text{dist}(\mathbf{y}_s, \Omega) \rightarrow \infty$$

proving the claim. \square

This resolution analysis implies the for any sampling points \mathbf{y}_s the imaging functional is strictly positive and will decay as \mathbf{y}_s moves away from the scatterer Ω . Therefore, one can plot $\mathcal{I}(\mathbf{y}_s)$ in order to recover the scatterer. Using the imaging functional $\mathcal{I}(\mathbf{y}_s)$ has the advantage that one does not have to solve an ill-posed equation at each sampling point. Other sampling methods such as the Linear sampling method [5] and Factorization method [12] requires one to solve a severely ill-posed equation involving the far field operator at each sampling point. This requires one to compute the singular-value decomposition of the far field operator as well as applying a regularization scheme. Also these methods could be sensitive to noise added to the scattering data where as the Direct sampling method only requires one to compute an inner-product and by the following theorem (see also [14]) we see that the imaging functional is stable with respect to noise added to the far field data.

Theorem 10 (stability estimate). *For all $\widehat{\mathbf{x}}, \mathbf{d} \in \mathbb{S}^2$, let $\mathcal{D}(\widehat{\mathbf{x}}, \mathbf{d}) := \mathbf{u}^\infty(\widehat{\mathbf{x}}, \mathbf{d})(\mathbf{d} \times \mathbf{p}) \times \mathbf{d}$ be the far field data in the imaging functional \mathcal{I} in (13). Denote by \mathcal{I}_δ the imaging functional where data \mathcal{D} is replaced by its noisy version \mathcal{D}_δ . Then*

$$\mathcal{I}(\mathbf{x}) - \mathcal{I}_\delta(\mathbf{x}) \leq C\|\mathcal{D} - \mathcal{D}_\delta\|_{L^2(\mathbb{S}^2 \times \mathbb{S}^2)^3}, \quad \text{for all } \mathbf{x} \in \mathbb{R}^3,$$

where C is a positive constant.

Proof. The proof is a direct application of the triangle inequality and the Cauchy-Schwarz inequality. \square

5 Numerical examples

We present in this section several numerical examples to validate the performance of the direct sampling method. The simulations were carried on a Quad Core 3.6 GHz machine with 32GB RAM and the implementation was done using the computing software Matlab. The synthetic data are generated by numerically solving the direct problem with the spectral solver studied in [16]. We solve the direct problem (4)–(5) with incident field

$$\mathbf{E}_{\text{in}}(\mathbf{x}, \mathbf{d}_j, \mathbf{q}) = ik(\mathbf{d}_j \times \mathbf{p}) \times \mathbf{d}_j e^{ik\mathbf{x} \cdot \mathbf{d}_j}, \quad j = 1, 2, \dots, N_{\mathbf{d}}$$

where $\mathbf{p} = (1/\sqrt{3}, -1/\sqrt{3}, 1/\sqrt{3})^\top$ and $N_{\mathbf{d}}$ is the number of directions \mathbf{d}_j that is specified below for each numerical example. Likewise we denote by $N_{\widehat{\mathbf{x}}}$ the number of points $\widehat{\mathbf{x}} \in \mathbb{S}^2$ where the far field pattern data are collected. The points $\widehat{\mathbf{x}}$ and \mathbf{d} that are chosen for generating the scattering data are almost uniformly distributed on \mathbb{S}^2 . As in Theorem 10 let

$$\mathcal{D}(\widehat{\mathbf{x}}, \mathbf{d}) = \mathbf{u}^\infty(\widehat{\mathbf{x}}, \mathbf{d})(\mathbf{d} \times \mathbf{p}) \times \mathbf{d}$$

be our synthetic far field data that has three components $\mathcal{D}_n, n = 1, 2, 3$, and \mathcal{D}_n can be considered as an $N_{\widehat{\mathbf{x}}} \times N_{\mathbf{d}}$ matrix. To consider noisy data, we add artificial noise to our synthetic data. More precisely, a complex-valued noise matrix \mathcal{N} containing random numbers that are uniformly distributed in the complex square $\{a + ib, |a| \leq 1, |b| \leq 1\} \subset \mathbb{C}$ is added to the data matrix \mathcal{D}_n . Denoting by δ the noise level, the noisy data matrix $\mathcal{D}_{n,\delta}$ is then given by

$$\mathcal{D}_{n,\delta} := \mathcal{D}_n + \delta \frac{\mathcal{N}}{\|\mathcal{N}\|_2} \|\mathcal{D}_n\|_2, \quad n = 1, 2, 3,$$

where $\|\cdot\|_2$ is the matrix 2-norm.

Performance of the method on noisy data (Figure 1). The first example is presented in Figure 1 where we focus on performance of the sampling method on data perturbed by different amounts of noise. The scatterers include an ellipsoid and a ball that are characterized by smoothly varying contrast $P(\mathbf{x})$. More precisely,

$$\begin{aligned} \Omega_1 &= \{\mathbf{x} \in \mathbb{R}^3 : |\mathbf{x} - \mathbf{x}_0|^2 < 0.35^2, \mathbf{x}_0 = (0.4, 0, 0.4)^\top\} \\ \Omega_2 &= \left\{ \mathbf{x} = (x_1, x_2, x_3)^\top \in \mathbb{R}^3 : \frac{(x_1 + 0.3)^2}{0.45^2} + \frac{x_2^2}{0.25^2} + \frac{(x_3 + 0.3)^2}{0.25^2} < 1 \right\} \\ P(\mathbf{x}) &= \begin{cases} \frac{1}{2} \exp\left(1 - \frac{0.35^2}{0.35^2 - |\mathbf{x} - \mathbf{x}_0|^2}\right), & \mathbf{x} \in \Omega_1 \\ \frac{1}{2} \exp\left(1 - \frac{1}{1 - \frac{(x_1 + 0.3)^2}{0.45^2} + \frac{x_2^2}{0.25^2} + \frac{(x_3 + 0.3)^2}{0.25^2}}\right), & \mathbf{x} \in \Omega_2 \\ 0, & \text{else.} \end{cases} \end{aligned}$$

Here we choose wave number $k = 12$ (the corresponding wavelength is about 0.52) and $N_{\widehat{\mathbf{x}}} \times N_{\mathbf{d}} = 325 \times 325$. In Figure 1 we also present 3D-visualizations of exact

and reconstructed geometry using isosurface in Matlab. The isovalue for the isosurface plotting is chosen to be 25% of the maximal value of the computed imaging functional \mathcal{I} . Even there are high levels of noise $\delta = 0.3$ and 0.8 in the far field data, we can easily see that the sampling method is able to provide reasonable reconstructions. The computed images are not very different for 30% and 80% amounts of noise in the data. The solid performance of the method on noisy data can be justified by the stability of the method that is discussed in Theorem 10.

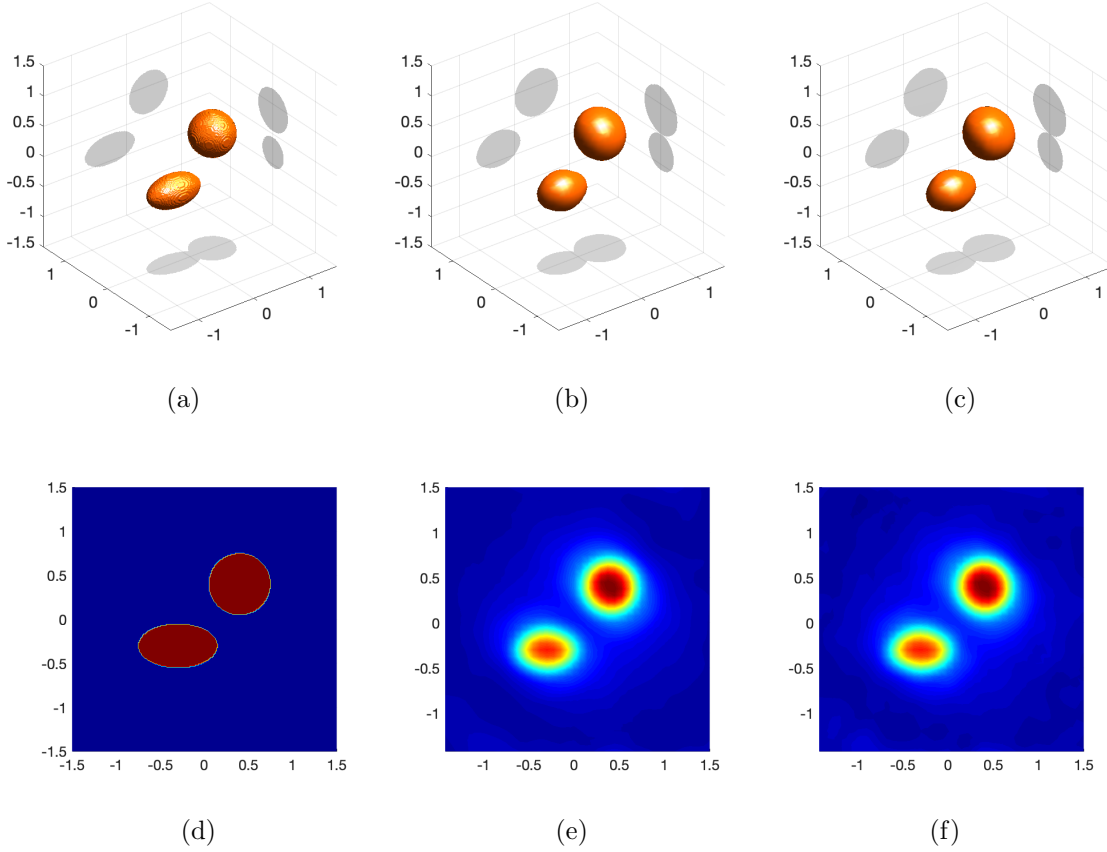


Figure 1: Reconstruction results with different levels of noise. The scatterers include an ellipsoid and a ball. $N_{\bar{\mathbf{x}}} \times N_{\mathbf{d}} = 325 \times 325$, wave number $k = 12$. (a) Exact geometry. (b) Reconstructed geometry for 30% noise ($\delta = 0.3$). (c) Reconstructed geometry for 80% noise. (d) Cross-sectional view of the exact geometry. (e) Cross-sectional view of the computed imaging functional \mathcal{I} for 30% noise. (f) Cross-sectional view of computed imaging functional \mathcal{I} for 80% noise. The isovalue in the isosurface plotting is 25% of the maximal value of the computed imaging functional \mathcal{I} .

Performance of the method on smaller amount of data and data with smaller wave number (Figure 2). This is the focus of the second example that is to examine the performance of the direct sampling method on a smaller wave number

and a smaller set of scattering data. We consider the same scatterers as in the first example with an ellipsoid and a ball. The data in this example are perturbed by 30% noise. We can see in Figure 2(b) that for $N_{\hat{\mathbf{x}}} \times N_{\mathbf{d}} = 325 \times 325$ and wave number $k = 6$ (wavelength is about 1.04) the reconstruction result is not as good as that of the case $k = 12$ (Figure 2(c)). Although we can see two components of the scatterers in the reconstruction the shape and locations are not very accurate. The result is even worse if we have less data, see Figure 2(d). More precisely, for $N_{\hat{\mathbf{x}}} \times N_{\mathbf{d}} = 91 \times 91$ and $k = 12$, the reconstruction is no longer reasonable.

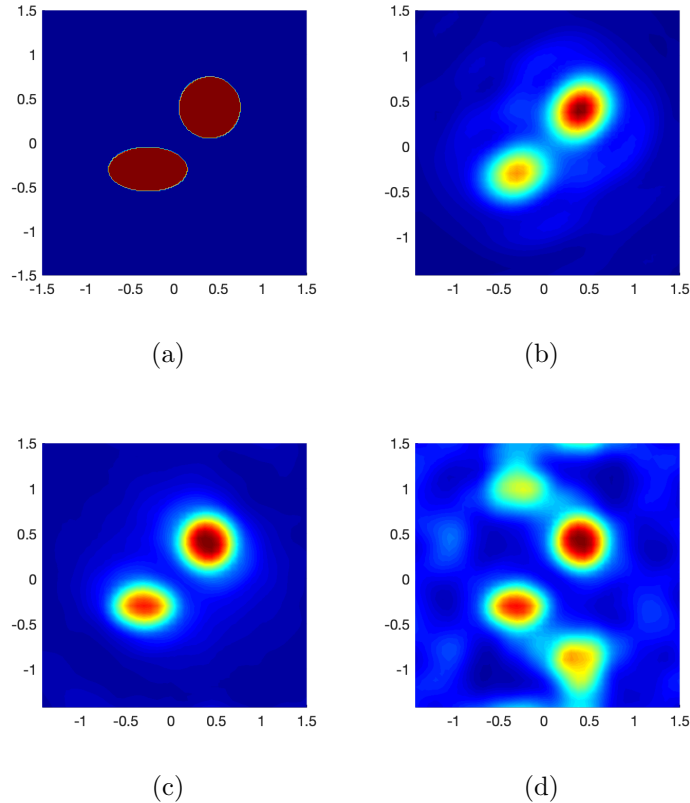


Figure 2: Reconstruction results with a smaller wave number and a smaller amount of scattering data in cross-sectional views of the computed imaging functional \mathcal{I} . There is 30% noise added to the data. (a) Exact geometry. (b) $N_{\hat{\mathbf{x}}} \times N_{\mathbf{d}} = 325 \times 325$ and $k = 6$. (c) $N_{\hat{\mathbf{x}}} \times N_{\mathbf{d}} = 325 \times 325$ and $k = 12$. (d) $N_{\hat{\mathbf{x}}} \times N_{\mathbf{d}} = 91 \times 91$ and $k = 12$.

Performance of the method for different types of scatterers (Figure 3). In the last example we present in Figure 3 the reconstruction results for different types of scatterers. We consider scatterers with more complicated shapes and non-smooth geometries. For the scatterer in Figure 3(a) the contrast $P(\mathbf{x})$ is again a smoothly

varying function defined by

$$\begin{aligned}\Omega_1 &= \{\mathbf{x} \in \mathbb{R}^3 : |\mathbf{x} - \mathbf{a}|^2 < 0.3^2, \mathbf{a} = (0, 0, 0.4)^\top\} \\ \Omega_2 &= \{\mathbf{x} \in \mathbb{R}^3 : |\mathbf{x} - \mathbf{b}|^2 < 0.5^2, \mathbf{b} = (0, 0, -0.3)^\top\} \\ P(\mathbf{x}) &= \begin{cases} \frac{1}{2} \exp\left(1 - \frac{0.3^2}{0.3^2 - |\mathbf{x} - \mathbf{a}|^2}\right), & \mathbf{x} \in \Omega_1 \\ \frac{1}{2} \exp\left(1 - \frac{0.5^2}{0.5^2 - |\mathbf{x} - \mathbf{b}|^2}\right), & \mathbf{x} \in \Omega_2 \\ 0, & \text{else.} \end{cases}\end{aligned}$$

The contrast $P(\mathbf{x})$ for the scatterers in Figure 3(b,c) is equal to 0.2 in Ω and 0 outside of Ω . The data in this example are again perturbed by 30% noise. The pictures show that with the right amount of data the sampling method is able to provide good reconstruction results for scatterers with more complicated shapes. We also observe that for scatterers with non-smooth geometries like in Figures 3(b) and (c), the isovalue in the isosurface plotting should be 50% of the maximal value of the computed imaging functional \mathcal{I} to give a better three-dimensional image.

Acknowledgement. The work of DLN is partially supported by NSF grant DMS-1812693.

References

- [1] L. Audibert and H. Haddar, A generalized formulation of the linear sampling method with exact characterization of targets in terms of far-field measurements, *Inverse Problems* **30** 035011 (2014).
- [2] T. Arens, Why linear sampling method works, *Inverse Problems* **20** (2004), 163-173 (2004).
- [3] T. Arens and A. Lechleiter, Indicator Functions for Shape Reconstruction Related to the Linear Sampling Method, *SIAM J. Imaging Sci.* **8(1)** (2015) 513-535.
- [4] F. Cakoni, D. Colton, and P. Monk, “*The linear Sampling Method in Inverse Electromagnetic Scattering*”, CBMS Series, SIAM Publications 80, (2011).
- [5] F. Cakoni, D. Colton, and H. Haddar, *Inverse Scattering Theory and Transmission Eigenvalues* CBMS-NSF Regional Conference Series in Applied Mathematics, SIAM 2016.
- [6] F. Cakoni and J. Rezac, Direct imaging of small scatterers using reduced time dependent data, *J. Comput. Phys.* **338** (2017) 371-387.
- [7] D. Colton and R. Kress. *Inverse Acoustic and Electromagnetic Scattering Theory*. Springer, New York, 3rd edition, 2013.

- [8] I. Harris and A. Kleefeld, Analysis of new direct sampling indicators for Far-field measurements. *Inverse Problems* **35** 054002 (2019)
- [9] H. Heck, G. Nakamura and H. Wang, Linear sampling method for identifying cavities in a heat conductor, *Inverse Problems*, **28** 075014 (2012).
- [10] X. Ji, X. Liu and Y. Xi, Direct sampling methods for inverse elastic scattering problems, *Inverse Problems* **34** 035008 (2018).
- [11] A. Kirsch, The factorization method for Maxwell's equations, *Inverse Problems* **20** S117–S134 (2004).
- [12] A. Kirsch and N.I. Grinberg. *The Factorization Method for Inverse Problems*. Oxford Lecture Series in Mathematics and its Applications 36. Oxford University Press, 2008.
- [13] K. H. Leem, J. Liu and G. Pelekanos, Two direct factorization methods for inverse scattering problems, *Inverse Problems* **34** 125004 (2018).
- [14] X. Liu, A novel sampling method for multiple multiscale targets from scattering amplitudes at a fixed frequency. *Inverse Problems*, **33** 085011 (2017).
- [15] P. Monk, “*Finite Element Methods for Maxwell's Equations*”, Oxford University Press, 2003.
- [16] D.-L. Nguyen, Direct and Inverse Electromagnetic Scattering Problems for Bi-Anisotropic Media. *Inverse Problems*, <https://doi.org/10.1088/1361-6420/ab382d>, 2019.
- [17] R. Potthast, A study on orthogonality sampling, *Inverse Problems* **26** 074075 (2010).
- [18] B. Schweizer, On Friedrichs Inequality, Helmholtz Decomposition, Vector Potentials, and the div-curl Lemma. *Trends in Applications of Mathematics to Mechanics*. Springer INdAM Series, vol 27. Springer, 2018.

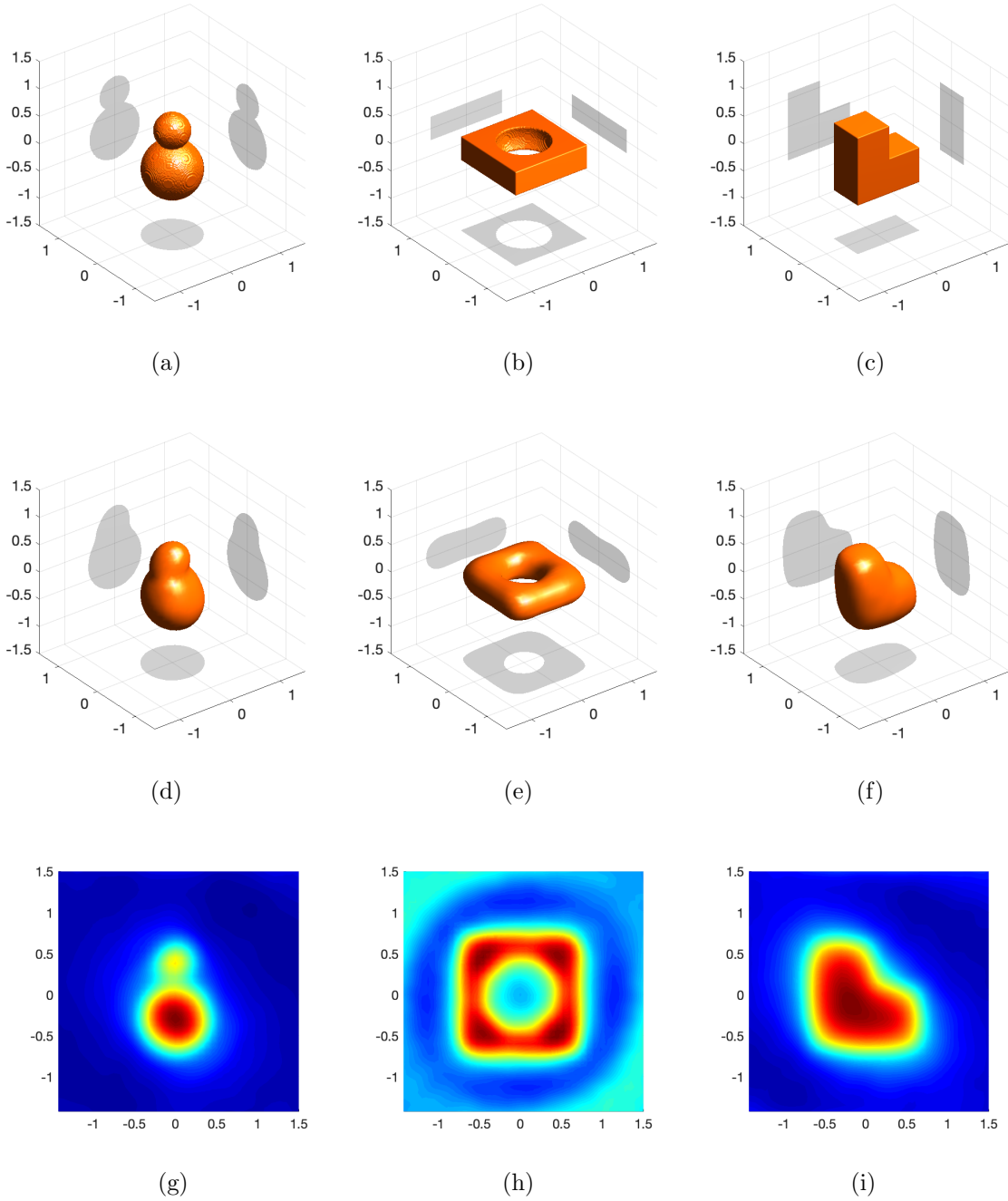


Figure 3: Reconstruction results for scatterers with more complicated shapes. There is 30% noise in the scattering data. The images in the first line and the second line are respectively the exact geometries of the scatterers and the corresponding reconstructed geometries. Cross-sectional views of the computed imaging functional \mathcal{I} are displayed in the last line. (d, g) $N_{\hat{\mathbf{x}}} \times N_{\mathbf{d}} = 231 \times 231$ and $k = 10$. (e, h) $N_{\hat{\mathbf{x}}} \times N_{\mathbf{d}} = 231 \times 231$ and $k = 12$. (f, i) $N_{\hat{\mathbf{x}}} \times N_{\mathbf{d}} = 325 \times 325$ and $k = 12$. The isovalues in the isosurface plotting are respectively 25% and 50% of the maximal value of the computed imaging functional \mathcal{I} for (d) and (e, f).